J. Phys. B: At. Mol. Opt. Phys. **21** (1988) 1545-1562. Printed in the UK

Density matrices of the $n = 2$ and 3 manifolds of H atoms produced in p–H collisions at 1–50 keV impact energies

Ashok Jain†, C D Lin† and W Fritsch‡

† Physics Department, Cardwell Hall, Kansas State University, Manhattan, KS 66506, USA
‡ Bereich Kern- und Strahlenphysik, Hahn-Meitner-Institute Berlin GmbH, D-1000 Berlin 39, Federal Republic of Germany

Received 9 September 1987, in final form 1 December 1987

Abstract. We study the full density matrices (differential as well as integrated with respect to impact parameter) for charge transfer and excitation to the $n = 2$ and 3 manifolds of the excited hydrogen atoms formed in p-H collisions over impact energies 1-50 keV. The scattering amplitudes are determined using the modified two-centre atomic-orbital-expansion method (AO+) based on the impact parameter formalism. From these scattering amplitudes several physical parameters such as the dipole moment, velocity vector, charge density and current distribution are extracted. The analysis of these parameters allows us to provide an approximate *classical* orbital picture for excitation and charge transfer to each manifold at both the low ($E < 5$ keV) and intermediate ($E > 20$ keV) energy regions. In general, we can interpret the charge distribution around each centre after the collision as resulting from the electron cloud being pulled apart between the two collision centres as they move away from each other. Comparison is also made with the electron charge density for the $n = 2$ manifold of H in electron-hydrogen and positron-hydrogen impact excitations at 50-200 eV using the calculation of van Wyngaarden and Walters.

1. Introduction

Recently, we calculated and analysed the full density matrices of the excited H ($n = 2$ and 3) atoms formed in proton-helium collisions at intermediate projectile velocities ($v \simeq 1$-2 au) (Jain *et al* 1986, 1987a, b). In addition to the capture cross sections to the *nlm* sublevels, several physical parameters such as dipole moment, velocity vector, probability and current densities of the electron charge cloud etc were deduced from the density matrix elements. The integrated (over the impact parameter b) density matrix elements and their various coherence parameters were found to be in fairly good agreement with values deduced from experimental measurements (Havener *et al* 1982, 1984, 1986, Westerveld *et al* 1987). To determine these parameters (or equivalently, the off-diagonal elements of the density matrix) experimentally it is necessary to measure the Stokes parameters for the light emitted in the presence of external axial and/or transverse electric fields. These measurements and theoretical studies explore coherence parameters of hydrogenic states, which are not obtainable from cross sections alone. These density parameters allow us to unravel more details of the collision dynamics. By examining the differential density matrix, we were able to provide a *classical* orbital picture of the electron after charge transfer (Jain *et al* 1986, 1987a, b).

While these studies were motivated originally by the experimental investigation, we recognise that the proton-helium collision system has several disadvantages compared with the theoretical viewpoint. Because of the complexity of a more realistic

two-electron treatment (see, e.g., Fritsch and Lin 1986), the independent particle approximation was used to describe the two electrons in the system. This limited the energy range where we could reliably study the density matrices. Furthermore, the excited states of helium atoms for a given n manifold are not degenerate so the coherences between states of different l (for a given n) do not exist. In order to explore the relations between coherence parameters of the target states and the projectile states, it is desirable to study one-electron collision systems where the density matrix and its coherence parameters on both centres can be examined simultaneously. In this paper the symmetric proton-hydrogen system is investigated.

The proton-hydrogen system has been studied extensively using various theoretical models within coupled-state formulations in the 1-75 keV region (for example, see Kimura and Lin (1985), Winter and Lin (1984) and Kimura and Thorson (1981) for details and earlier references). Only excitation and capture cross sections to the $n=2$ manifolds were addressed in these calculations (except the work by Rapp and Dinwiddie (1972) who have reported the p-H capture and excitation cross sections only for 3s, $3p_0$ and $3p_1$ states of the $n=3$ manifold in their seven-state AO expansion close-coupling calculations). These extensive calculations in general are in good agreement with the experimental measurements. This system has also been studied by Fritsch and Lin (1982, 1983a, b) using the so-called AO+ model: this is a modification of the conventional two-centre atomic-orbital (AO) expansion method where suitable pseudostates were included in addition to the bound excited orbitals of the target and of the projectile atoms. In the low-energy region the pseudostates were chosen to be the atomic orbitals of the united atom to account for the molecular binding effects expected at low energies, and in the higher-energy region where ionisation channels are important the pseudostates were chosen to be the discretised continuum states. In this way, the AO+ method allows us to study the p-H collisions over a broad energy range and cross sections from these calculations have been found to be in good agreement with other calculations and with experiments (Fritsch and Lin 1983a, b). With these previously tested results in mind, in this paper we extract additional physical parameters from the calculated scattering amplitudes obtained by the AO+ model and investigate the interrelations of these parameters between the excitation and charge transfer channels to provide further analysis of the collision dynamics.

A complete description of an ion-atom collision experiment is the specifics of scattering amplitudes or, equivalently, the whole density matrix. The diagonal elements of the density matrix describe the scattering cross sections while the off-diagonal matrix elements describe coherences between the final states. In reality, only the coherences between degenerate and near-degenerate states can be measured directly. Therefore the coherences between the magnetic sublevels have been extensively studied in both electron-atom and in ion-atom collisions. These coherences can be expressed in terms of off-diagonal matrix elements or in terms of multipole moments (Blum 1981, Fano and Macek 1973). For one-electron atoms, the states within a given n manifold are nearly degenerate and the coherences among these states can be measured in an external electric field (Havener *et al* 1986). Because of the large number of elements in the density matrix in a given n manifold, attempts have been made to extract a few physically meaningful quantities from the density matrix for a given n manifold (Gabrielse and Band 1973, Burgdörfer 1983, Havener *et al* 1984, 1986). In our previous p-He work (Jain *et al* 1986, 1987a, b), we used the first-order moments (dipole moment arising from the real parts of the off-diagonal elements, velocity vector ($\boldsymbol{L}\times\boldsymbol{A}$) due to coherences between imaginary parts of the off-diagonal components) and the

three-dimensional and contour plots of probability and current distributions of the differential as well as of the averaged density matrix. In this paper we perform the same analysis for both the target excitation and projectile capture states in proton-hydrogen collisions. The various moments on the target and on the projectile are examined to reveal the shape of the electron cloud on each centre after the collision and the results are interpreted in terms of the charge cloud evolution during the collision.

Theoretical study of the full density matrices for the excitation of the $n=2$ and 3 manifolds of H atoms under proton impact at velocities 1-5 au has been carried out recently by Schöller *et al* (1986). These authors used the first Born and the one-centre (target-centred) AO expansion methods in order to calculate the density matrix and its various parameters. Since charge transfer channels were not included in their AO expansion, as noted by Schöller *et al* their results are expected to be valid only at higher energies ($v/v_e \geqslant 2.0$ au). Similarly, for charge transfer at high velocities, Burgdörfer (1986) discussed the p-H density matrix in terms of statistical multipoles in the continuum-distorted-wave (CDW) approximation. Again the CDW theory is also a high-energy approximation and therefore not suitable in the energy range of interest here. Thus, the present study is the first one to address the density matrices and coherence parameters for both the excitation and charge transfer channels simultaneously for p-H collisions in the 1-50 keV region.

We also discuss the density matrix parameters and the *classical* orbital picture for the case of electron (and positron) impact excitations of hydrogen atoms ($n=2$ manifold) at intermediate energies (50-200 eV) from the calculations of van Wyngaarden and Walters (1985). In the next section, a summary is given of the theoretical and numerical methods. Section 3 presents our results and discussion. The concluding remarks are made in § 4. We use atomic units throughout unless otherwise specified.

2. Theoretical and numerical methods

2.1. Calculation of transition amplitudes and partial cross sections

The capture and target excitation amplitudes, $a_{nlm}(b)$, are calculated in the present investigation using the close-coupling method with a two-centre basis set (Fritsch and Lin 1982, 1983a, b). Two sets of basis functions were employed, each consisting of a total of 28 states. The basis set I was chosen for representing the physical excitation mechanism in the higher-energy region ($E > 15$ keV), and set II for the lower-energy region ($1 < E < 15$ keV). In set I, there are 14 functions on each centre. They include the ten $n=1, 2$ and 3 states of the hydrogen atom in the separated-atom limit, and four pseudostates to represent the ionisation channels partially (Fritsch and Lin 1983b). In the low-energy region, we consider the excitation and charge transfer to the $n=2$ states only. (The $n=3$ cross sections are quite small as compared with $n=2$ values.) Note that the effect of $n=3$ manifold on the $n=2$ cross sections is not significant (see also Rapp and Dinwiddie 1972). To account for the molecular behaviour for collisions at low energies in an atomic-orbital expansion method, united-atom orbitals were included in the basis set II (Fritsch and Lin 1982). Recognising that the 3d molecular orbital correlates to the 2p separated-atom limit, in basis set II we include the 1s, 2s, 2p and 3d states of both separated-atom and united-atom orbitals on each centre in the calculation. As mentioned earlier the main purpose of this work is to study the behaviour of the electronic charge cloud and other coherence parameters after the collision around the two centres, therefore, we will not present cross sections to each

excitation and charge transfer channel except mentioning here that they are in accord with the previous calculations of Fritsch and Lin (1982, 1983b).

2.2. Integrated density matrices and multipole moments

The details on the theory and symmetry properties of the differential density matrix and the definition of its various physical parameters including probability and current distributions are already given in the literature (Burgdörfer 1983, Havener *et al* 1986, Jain *et al* 1987b). First we discuss the integrated (over b) density matrices and their first-order moments for both the capture and target excitation cases as they are more readily determined experimentally (Havener *et al* 1986).

Figures 1 and 2 display the energy dependence of the normalised coherence parameters $\langle D_z\rangle^{\text{cap}}, \langle D_z\rangle^{\text{exc}}, \langle(\boldsymbol{L}\times\boldsymbol{A})_z\rangle^{\text{cap}}$ and $\langle(\boldsymbol{L}\times\boldsymbol{A})_z\rangle^{\text{exc}}$ for both the $n=2$ and 3

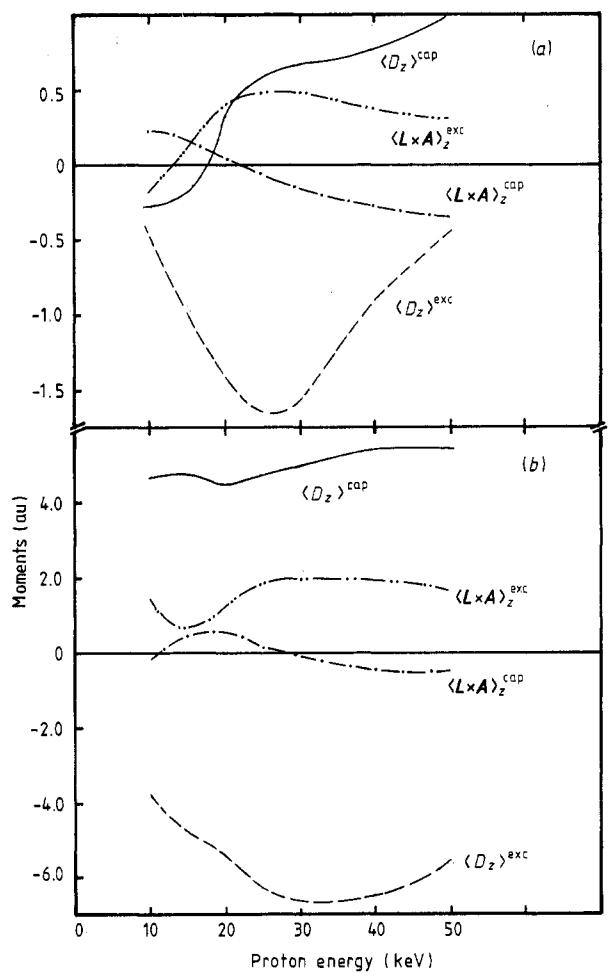

Figure 1. Normalised dipole moments $\langle D_z\rangle$ and velocity vector $(\boldsymbol{L}\times\boldsymbol{A})_z$ for $n=(a)$ 2 and (b) 3 manifolds for both the capture and target excitation processes in p–H collisions using the 28-state basis set I (see text for details) in the range 15–50 keV. Each curve is labelled accordingly.

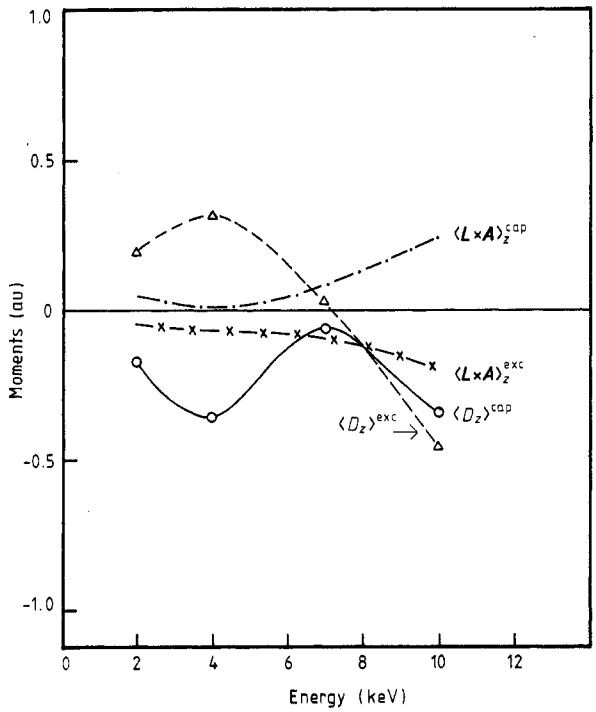

Figure 2. Same as in figure 1, but for $n = 2$ in the 2-10 keV energy range using the 28-state basis set II (see text for details).

manifolds. We remind the reader that $\langle D_z\rangle$ is the integrated (over impact parameters) dipole moment for a given manifold along the direction of the incident beam (the z axis), and $\langle(\boldsymbol{L}\times\boldsymbol{A})_z\rangle$ corresponds to the integrated *classical* Kepler velocity (along the z axis) at the perihelion. For our purpose here we will call $\langle D_z\rangle$ the dipole moment, and $\langle(\boldsymbol{L}\times\boldsymbol{A})_z\rangle$ the velocity vector at the perihelion. We emphasise that these quantities shown in figures 1 and 2 are normalised; i.e. they were divided by the total cross section for each corresponding manifold and centre.

We first concentrate on the results in the higher energy region. In figure 1 we notice that for $E > 20$ keV the dipole moments are positive for capture and negative for excitation channels, for both the $n = 2$ and 3 manifolds. This indicates that the electron cloud is lagging behind the projectile nucleus for capture processes and ahead of the target nucleus for excitation events. This is consistent with the total electronic density plots, for example for the α-H charge transfer collisions, where the electron charge cloud is seen to be lagging behind the projectile and ahead of the target centre (Winter *et al* 1985). We can perceive that this results from the break-up of the electron charge cloud between the two collision centres as the two centres are moving apart from each other. The positive dipole moments for electron capture processes at higher collision energies are consistent with the experimental data obtained for p-He collisions (Havener *et al* 1986) and with theoretical calculations (Burgdörfer and Dubé 1984, Jain *et al* 1987b). For $E > 30$ keV, the velocity vectors at the perihelion are negative for capture for both $n = 2$ and 3 shells and are positive for excitations. This implies classically that at these energies the electronic currents are of opposite sense for the target and projectile.

At low impact energies (for example below 20 keV for the $n=2$ manifold) the dipole moment for capture becomes negative and at still lower energies we see an oscillatory behaviour of the dipole moment. A more detailed graph displaying the dipole moments and the velocity vector at the perihelion is shown in figure 2 for the $n=2$ manifold for both excitation and capture channels. At these lower energies the corresponding quantities for capture and for excitation channels are of opposite signs compared with the results shown at high energies (figure 1). For energies around 8 keV, the behaviour of density matrix parameters is more complicated. Since the quantities in figure 1 and 2 are integrated over impact parameters, we postpone the detailed analysis until the next subsection.

From the density matrices it is also possible to extract the electronic charge cloud distribution and current flow around each centre. As an example, we display three-dimensional plots for the charge density in figure 3. The two graphs of the upper frame give the charge density plots for $n=2$, where the electron cloud is indeed in front of the target centre for excitation, and behind the projectile centre for charge transfer. The front-end asymmetry is quite obvious. A similar situation can be seen in this figure for the $n=3$ manifold. In fact, this general behaviour can be expected for other higher n levels and for low-energy continuum electrons (Burgdörfer 1986, Schöller *et al* 1986). The 'coherence' between excitation and charge transfer exists not only in the charge density, but in the current distribution also. In figure 4 we note that the sense of the current for capture is opposite to that for excitation for both the $n=2$ and 3 manifolds, while for a given centre the sense of current is independent of n. These behaviours, although shown for 50 keV only, are typical of collisions at other higher energies too.

At present, there are no experimental data or other calculations available for comparison with our results. The calculation of Schöller *et al* (1986) considered the excitation channels only in a one-centred atomic-orbital expansion method. They employed ten orbitals (corresponding to $n=1$, 2 and 3 levels) at the target and reported various state multipoles of the density matrix. We repeated their one-centre results by employing 10, 14 and 20 states at the target. The extra orbitals (pseudostates) in our 14- and 20-state sets represented the continuum. Unfortunately, we could not reproduce their ten-state density matrix elements. Our one-centre 14- and 20-state results for the dipole moments and velocity vectors are consistent with the present two-centre AO+ data; however, the ten-state results show positive values of the dipole moments for all the energies considered by Schöller *et al.* We therefore feel that a one-centred calculation without taking into account the coupling with continuum channels may not be sufficient even for a qualitative picture of the target excitation. (Note that the ionisation cross sections are quite large at these energies.) We would therefore not consider the results of Schöller *et al* further in our discussion. Calculations by Burgdörfer (1985) were limited to the continuum-distorted-wave approximation for the charge transfer channel only, which is also designed for collisions at higher energies and moreover it does not treat the excitation and charge transfer together.

2.3. Differential density matrix and its moments

We first discuss our results at the lower end of our energy regime, calculated using the basis set II (see § 2.1). Shown in figure 5 are the x and z components of the dipole moment vector $\boldsymbol{D}(b)$ (the y axis being perpendicular to the x-z collision plane) and

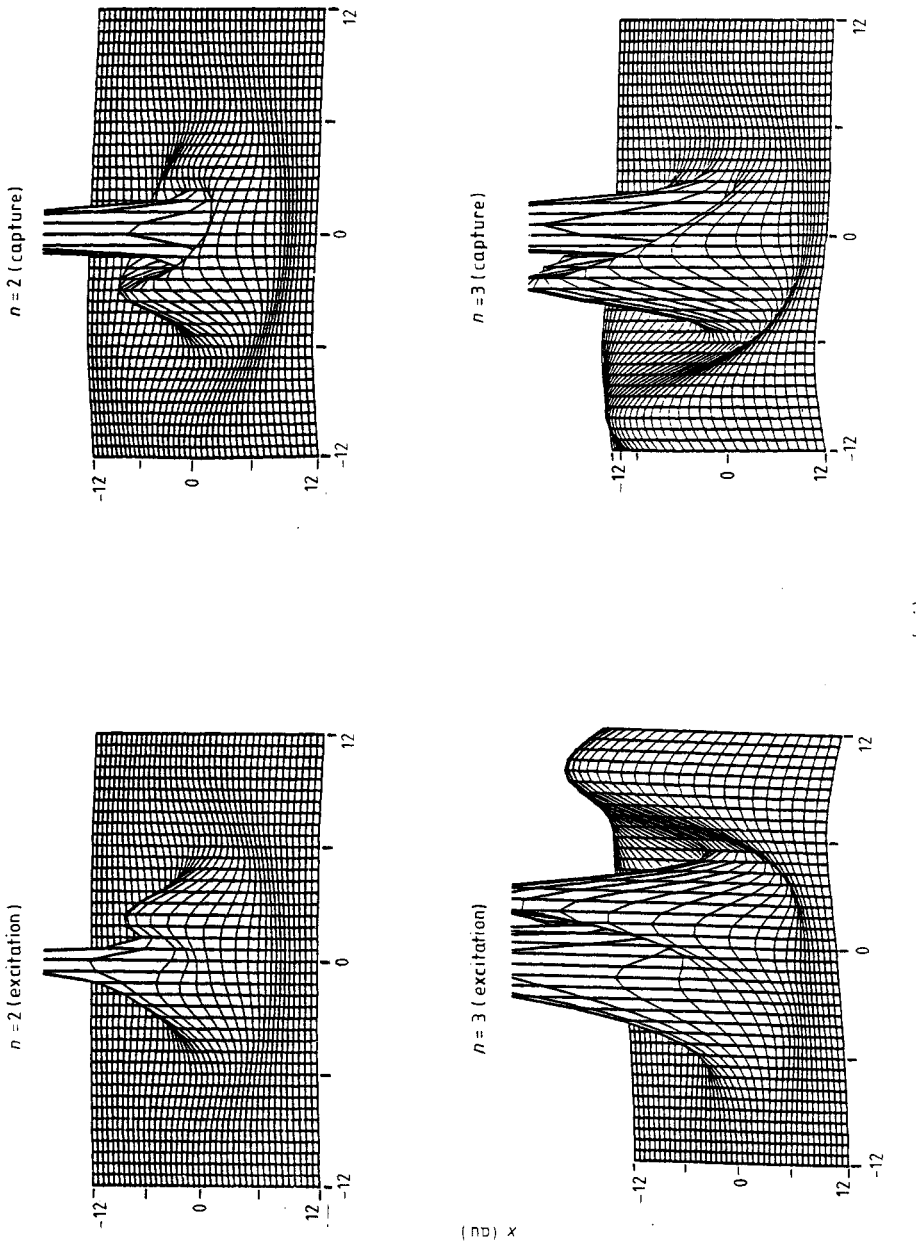

Figure 3. Electron probability distribution for excited H ($n = 2$) atoms formed in p–H collisions at 50 keV. Both the capture and excitation channels are illustrated.

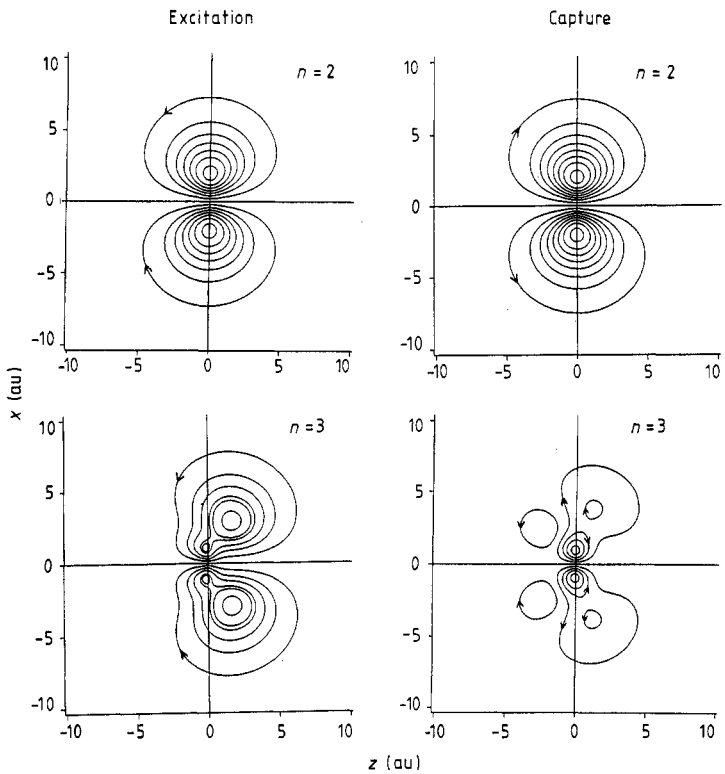

Figure 4. Electronic current distribution of the $n=2$ and 3 excited H atoms emerging from p-H collisions at 50 keV impact energy. The flow lines separate equal flows weighted by the distance from the z axis, i.e. equal amounts of $\sqrt{(x^2+y^2)}j$.

$(\boldsymbol{L}\times\boldsymbol{A})_z$, the z component of the velocity vector at the perihelion for $E=2$ and 4 keV. Except for the small 'irregularities' at larger impact parameters where the magnitude is quite small, note that the sign of each quantity for transfer is opposite to that for excitation. Note also that the magnitude of D_x is much larger than the magnitude of D_z. This is from the fact that the $2p_1$ cross sections are much larger than the corresponding 2s or $2p_0$ values since, at low energies, rotational coupling between $2p\sigma_u$ and $2p\pi_u$ is primarily responsible for the formation of $2p_1$ states (Ferguson 1961, Bates and Williams 1964). The opposite phases in D_x for charge transfer and excitation imply that the final charge distribution is the result of the charge cloud perpendicular to the internuclear axis (the $2p_1$ state) being pulled apart as the two centres are moving away from each other. Note that the results of the semiclassical close-coupling calculation shown in figure 5 are consistent with the approximate *classical* Kepler orbitals displayed in figure 6. We emphasise that the *senses* of rotation in the two orbits are the same. This orbital behaviour is characteristic of low-energy collisions.

We show the b dependence of D_z, D_x and $(\boldsymbol{L}\times\boldsymbol{A})_z$ for collisions at 25 and 50 keV in figure 7 for $n=2$ and in figure 8 for $n=3$. There are a number of points worth mentioning from these graphs: (1) the sign of D_z is always positive for capture and negative for excitation, implying that the charge cloud is lagging behind for capture and is ahead for the excitation case; (2) the sign of D_x changes for capture (both for

$n=2$ and $n=3$) from positive values at small impact parameters to negative values at large impact parameters, while for excitation the value of D_x is always positive, (3) there is also a sign change for $(\boldsymbol{L}\times\boldsymbol{A})_z$ for capture but not for excitation; (4) the impact parameter dependence for each quantity is nearly independent of n manifolds considered in this work. These properties reflect the fact that the *mechanism* for excitation (capture) to $n=2$ is similar to that for $n=3$. The results of figure 7 and 8 can be illustrated in terms of *classical* Kepler orbits. This is done in figure 9 for both the target and projectile centres at small and large b values. Note the orientation and sense of rotation of each orbit shown in figure 9.

The schematic classical orbits shown in figure 9 can be 'proved' by displaying the charge density in three-dimensional plots. They are shown in figure 10 for $n=2$ and in figure 11 for $n=3$. Note that in going from a small impact parameter ($b=1.3$) to

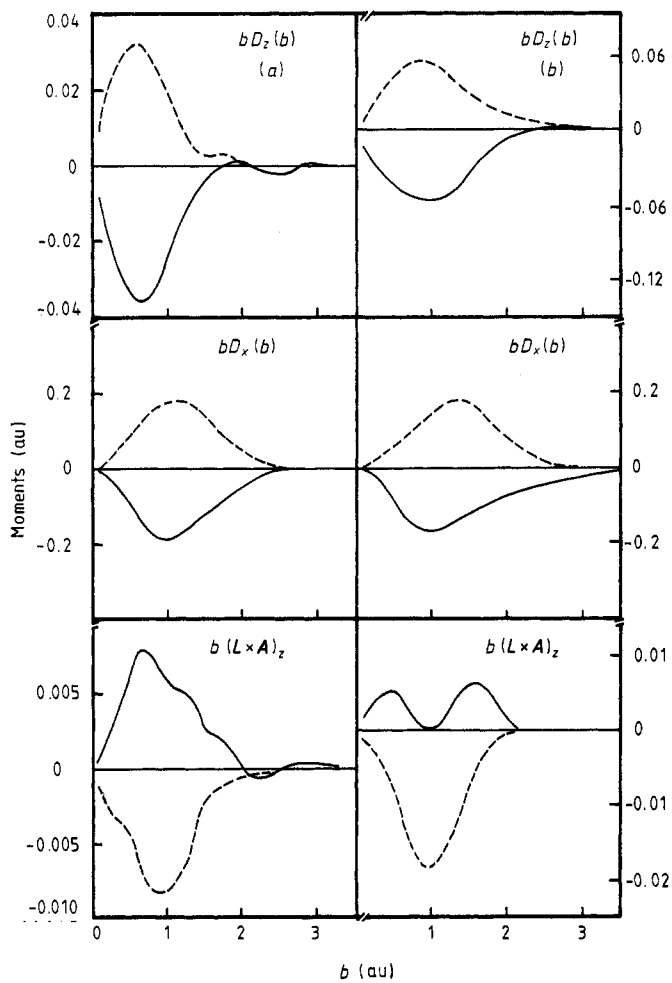

Figure 5. Present results on the impact-parameter-dependent dipole vector $\boldsymbol{D}(b)$ (x and z components) and $(\boldsymbol{L}\times\boldsymbol{A})_z$ for both capture (full curves) and excitation (broken curves) at (a) 2 and (b) 4 keV using the 28-state (see text for details) AO+ orbitals for the $n=2$ manifold.

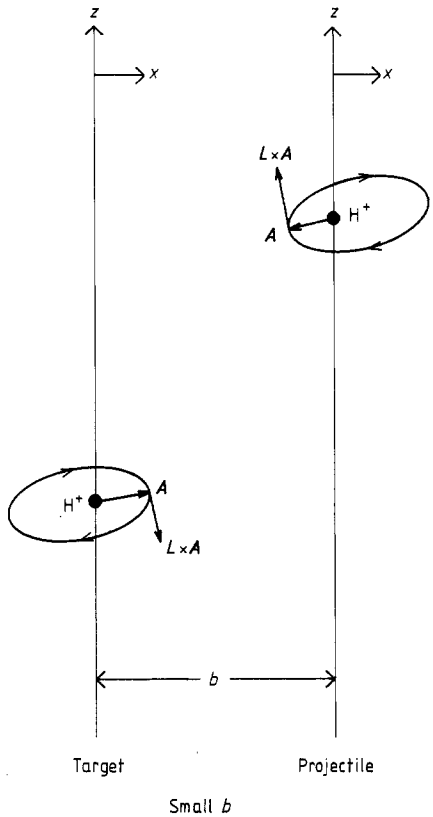

Figure 6. A classical orbital picture of the captured electron at low energies (below 10 keV).

a large one ($b = 2.8$), the charge cloud for excitation remains in the same 'location', while for capture it has changed from negative x at $b = 1.3$ to positive x at $b = 2.8$. These plots, resulting from quantal calculations, confirm the *classical* pictures derived from D_x, D_z and $(\boldsymbol{L} \times \boldsymbol{A})_z$ calculations shown in figure 9.

3. Density matrices for electron and positron impact excitation of the hydrogen atom

In this paper we have addressed the density matrices for the excited states of hydrogen on both the projectile and the target centres in p–H collisions. It is interesting to compare the coherence parameters in the corresponding electron (and positron) impact excitation of hydrogen atoms. Experimentally, electron–photon coincidence measurements have been performed for e–H collisions in an axial electric field (Back *et al* 1984). From the polarisation of Lyman-α radiation, the coherence between 2s and 2p states has been measured (Back *et al* 1984). Theoretically, such parameters have been calculated (van Wyngaarden and Walters 1985) using a multi-pseudostate close-coupling method. Their method, in fact, is similar to the AO+ model used in this work except that it treats the incident electron quantum mechanically and the expansion is

around the target centre only, while in the AO+ case, the motion of the projectile is described classically and the expansion is around both the target and the projectile centres. In other words, both methods treat the final-state interaction correctly.

We first discuss the electron impact case. The differential density matrices for the $n=2$ manifold in e-H impact excitation have been presented by van Wyngaarden and Walters (1985) at a number of collision energies. From their tables, we plot (in their notation) the $\mathrm{Re}(\mathrm{sp}_0^*)$ (proportional to D_z), $\mathrm{Re}(\mathrm{sp}_1^*)$ (proportional to D_x) and $\mathrm{Im}(\mathrm{sp}_0^*)$ (proportional to $(\boldsymbol{L}\times\boldsymbol{A})_z$) and display them graphically in figure 12 for the electron impact energy 54.4 eV ($v=2$ au). First we concentrate on small angles (or large impact parameters). Here D_z is positive and D_x is negative and $(\boldsymbol{L}\times\boldsymbol{A})_z$ is positive. By comparing with the corresponding values for excitations in p-H at 50 keV (see figure 7, right-hand column), we note that the sense of rotation is reversed between the two collision systems. This can be understood qualitatively in terms of the final-state interaction between the projectile and the target. In the case of p-H collision, the residual force on the target electrons by the projectile (including the electrons around

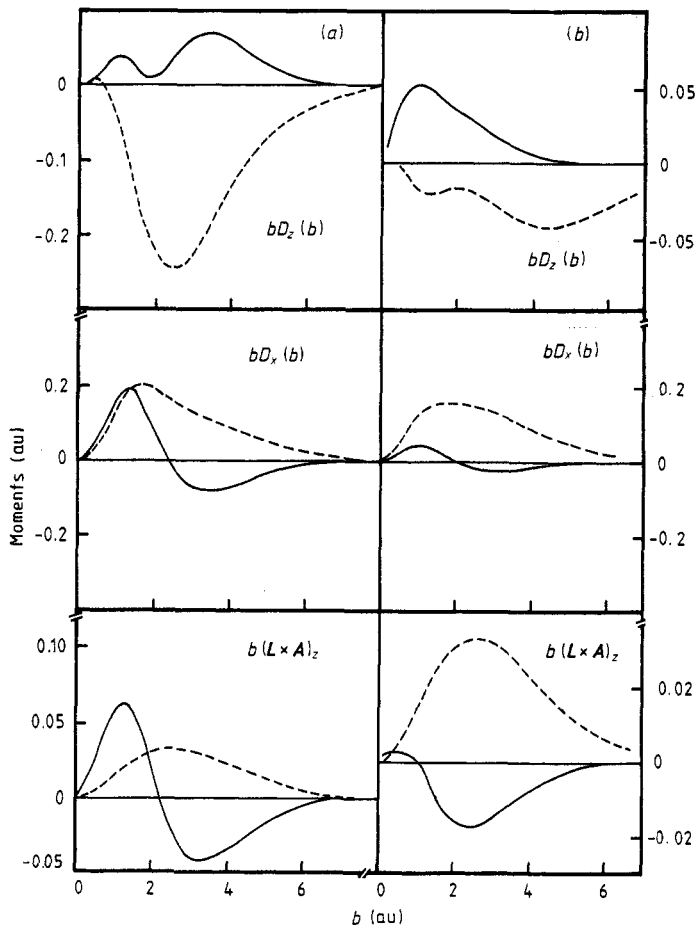

Figure 7. Same as in figure 5 except at higher energies ((*a*) 25 and (*b*) 50 keV) and using the 28-state AO+ basis set I.

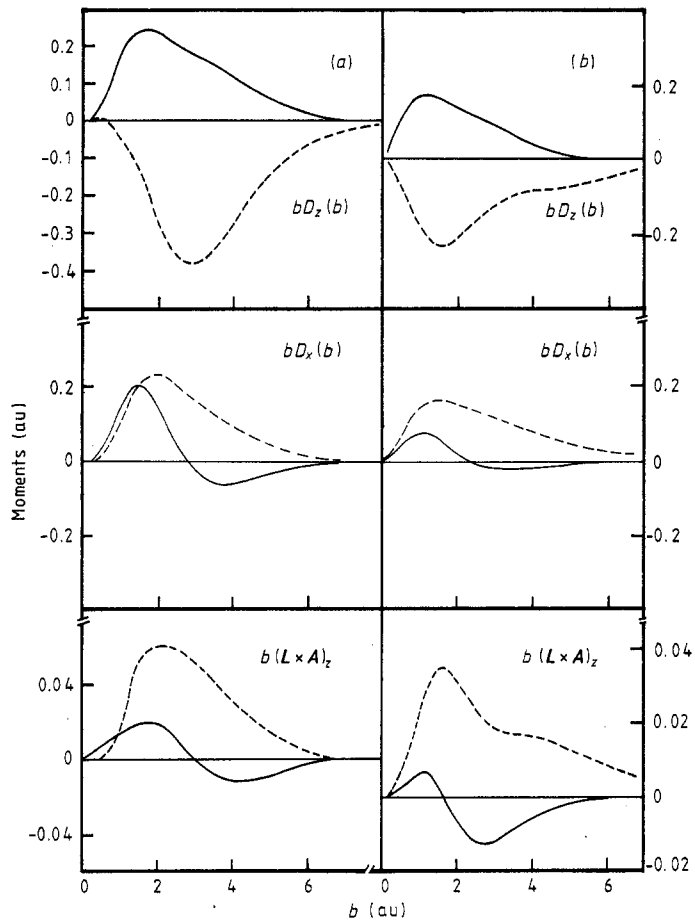

Figure 8. Same as for figure 7, except for the $n=3$ manifold.

the projectile) is attractive so that the electron cloud around the target tends to stay at the projectile side ($+z$ direction), while for e–H collision, the electron cloud experiences a repulsive force from the retrieving incident electron such that the atomic electron cloud tends to stay on the far side of the target. At larger angles where the incident electron is scattered backward (neglecting the exchange interaction) the excited electron cloud again pointing away from the retrieving scattered electron.

From figure 12 we can also sketch a *classical* orbital picture for the final $n=2$ states of H after electron impact excitation. They are shown in figure 13, one for small scattering angles and another for large scattering angles. The classical orbital pictures show the relative size of the dipole moments in the x and z direction and also the sense of the electronic orbit. The sense of rotation of the charge cloud changes sign going from the small angular region to large angles. This is equivalent to the sign changeover of the $\langle L_y\rangle$ parameter (defined as $\langle L_y\rangle = 2\sqrt{2}\,\mathrm{Im}(a_{210}a^*_{211})$), from positive values at small angles to negative values at large angles (see Madison and Winters 1981).

For the positron case, the corresponding quantities ($\mathrm{Re}(\mathrm{sp}^*_0)$, $\mathrm{Re}(\mathrm{sp}^*_1)$ and $\mathrm{Im}(\mathrm{sp}^*_0)$) are plotted in figure 14 from the calculations of Walters (1987). The *classical* orbital

picture derived from figure 14 is depicted in figure 15. Here the sense of current remains unchanged while going from small angles to large angles. This is equivalent and consistent with the negative values of the $\langle L_y \rangle$ parameter at all scattering angles in the case of target excitation by positrons (Madison and Winters 1981). Thus, the positron and the proton collisions both give rise to a similar rotation of the charge cloud at all angles, while for the electron there is a change in the sense of rotation from small to large angles.

4. Concluding remarks

We have studied theoretically the full density matrices of the excited H ($n = 2$ and 3 manifolds) atoms emerging from p–H collisions over the energy range 1–50 keV. A modified two-centre atomic-orbital (AO+) expansion approach within the impact parameter formalism is employed to evaluate the scattering amplitudes for target excitation and charge transfer channels. The density matrices for both $n = 2$ and 3 states for each centre are analysed in terms of various coherence parameters. We found that above 15 keV, the electron lags behind the projectile, while it is in front of the target. This is consistent with the intuitive picture that the electron cloud lying between the two centres splits as the two centres separate from each other. A classical picture of the electron's orbits around both centres is presented from the analysis of the differential density parameters.

At low energies ($E < 8$ keV), however, we found a different picture than at intermediate energies. In this low-energy domain, the integrated parameters reveal a situation where the electronic distribution is in front of the projectile (negative $\langle D_z \rangle$) and lagging

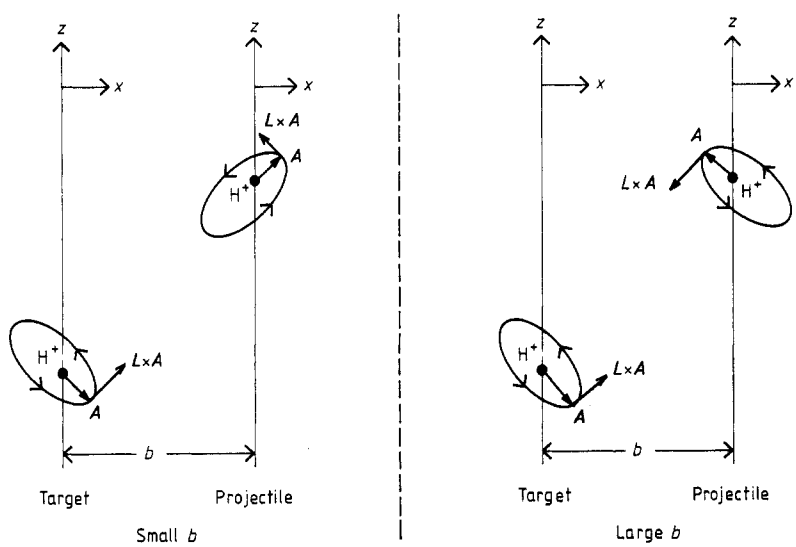

Figure 9. A classical orbital picture of the electron for the excitation (around the target) and capture (around the projectile) processes in the intermediate-energy ($E > 15$ keV) p–H collisions at (*a*) small *b* and (*b*) large *b* values.

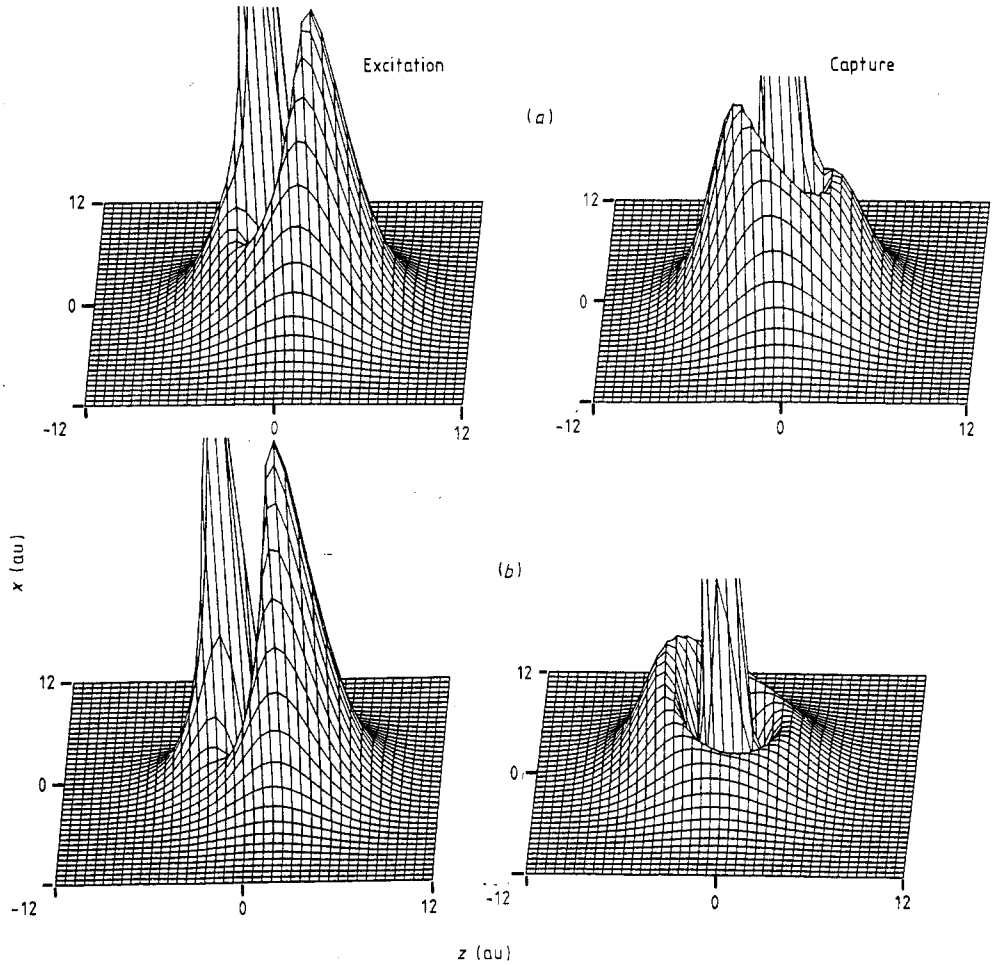

Figure 10. b-dependent differential probability density distribution of the charge cloud of H ($n = 2$) atoms emerging from the p-H collisions at 25 keV for (a) $b = 1.3$ and (b) 2.8 (au). Note that each plot is weighted arbitrarily in order to expose its hidden structures.

behind the target (positive $\langle D_z \rangle$). This picture is further discussed with respect to b-dependent dipole and velocity vectors in terms of the *classical* orbits around the target and the projectile centres. Here, it is more appropriate to think in terms of the dissociation of electronically excited $2p\pi$ of the H_2^+ molecular orbital into two atomic 2p orbitals as the two centres split. We have also analysed the calculated H ($n = 2$) differential (in angles) density matrices for electron and positron impact excitation of the hydrogen atom to extract D_x, D_z and $(\boldsymbol{L} \times \boldsymbol{A})_z$ to compare with the corresponding quantities in the excitation to $n = 2$ in p-H collisions.

Experimental data for most of the quantities described in the present paper are not available at this time. We also hope that this paper will stimulate similar studies from other theoretical models.

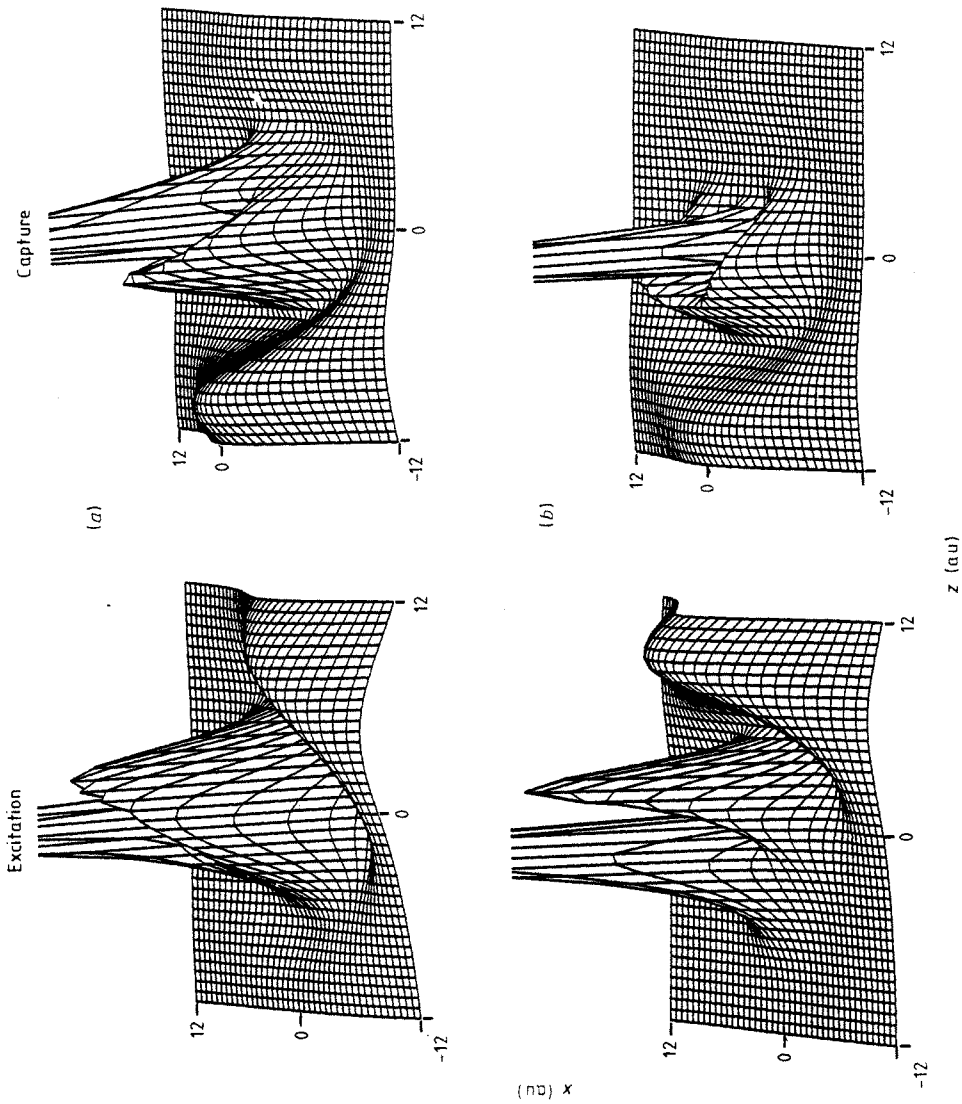

Figure 11. Same as in figure 10 except for the $n = 3$ manifold.

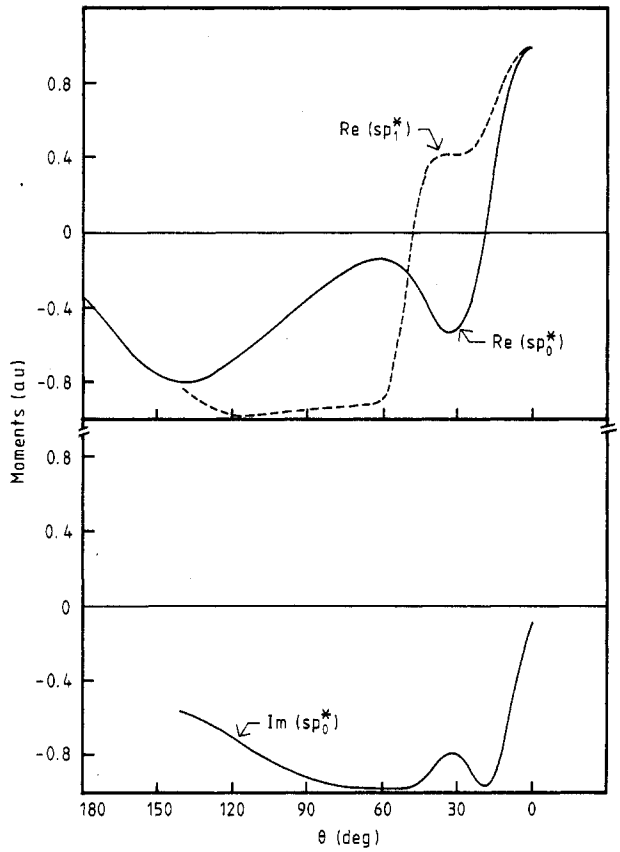

Figure 12. The quantities Re(sp$_0^*$) (proportional to D_z), Re(sp$_1^*$) (proportional to D_x) and Im(sp$_0^*$) (proportional to $(\boldsymbol{L}\times\boldsymbol{A})_z$) as a function of scattering angle θ. All the numbers are taken from van Wyngaarden and Walters (1985) for the excitation of H atoms by 54.5 eV electrons.

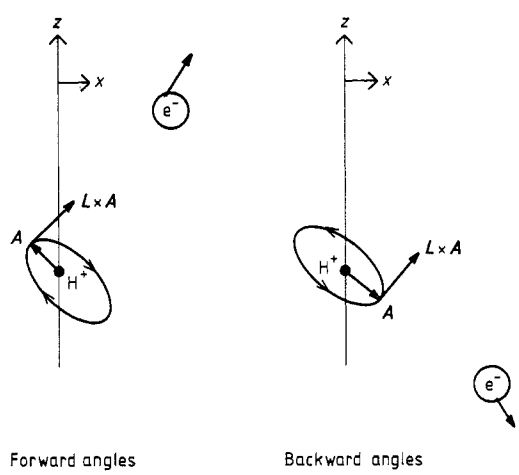

Figure 13. A classical picture of the electronic orbit around the target H atoms after e-H collisions.

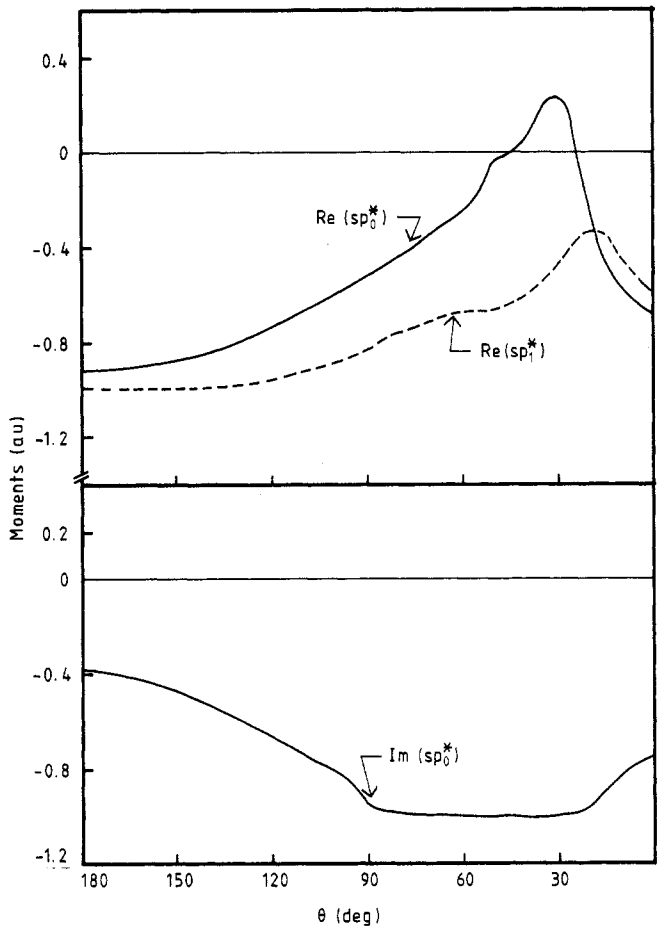

Figure 14. Same as in figure 12, but for the positron-hydrogen case at 54.5 eV energy. Data taken from Walters (1987).

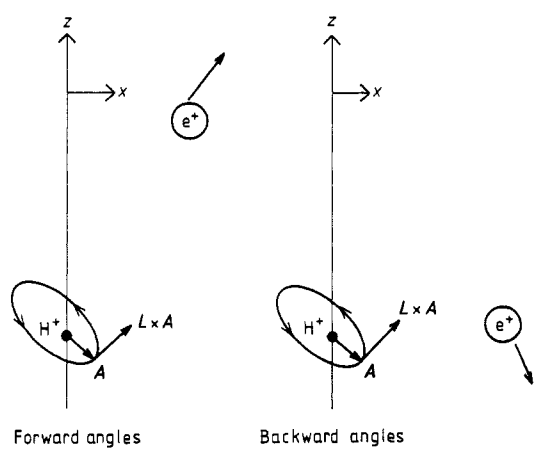

Figure 15. Same legend as in figure 13, but for the positron-hydrogen case.

Acknowledgment

We are indebted to William Westerveld for his help in making the contour plots of figure 4. Stimulating discussions with W Westerveld, C C Havener, D H Madison and Jiang Tan are gratefully acknowledged. We also thank H R J Walters for sending his positron data prior to publication. This work was supported in part by the US Department of Energy, Office of Energy Research, Division of Chemical Sciences.

References

Back C A, Watkins S, Eminyan M, Rubin K, Slevin J and Woolsey J M 1984 *J. Phys. B: At. Mol. Phys.* **17** 2695
Bates D R and Williams D A 1964 *Proc. R. Soc.* A **83** 425
Blum K 1981 *Density Matrix Theory and Applications* (New York: Plenum)
Burgdörfer J 1983 *Z. Phys.* A **309** 285
—— 1986 *Phys. Rev.* A **33** 1578
Burgdörfer J and Dubé L J 1984 *Phys. Rev. Lett.* **52** 2225
Fano U and Macek J 1973 *Rev. Mod. Phys.* **45** 553
Ferguson A F 1961 *Proc. R. Soc.* A **264** 540
Fritsch W and Lin C D 1982 *Phys. Rev.* A **26** 762
—— 1983a *J. Phys. B: At. Mol. Phys.* **16** 1595
—— 1983b *Phys. Rev.* A **27** 3361
—— 1986 *J. Phys. B: At. Mol. Phys.* **19** 2683
Gabrielse G and Band Y B 1973 *Phys. Rev. Lett.* **45** 553
Havener C C, Rouze N, Westerveld W B and Risley J S 1984 *Phys. Rev. Lett.* **53** 1049
—— 1986 *Phys. Rev.* A **33** 276
Havener C C, Westerveld W B, Risley J S, Tolk N H and Tully J C 1982 *Phys. Rev. Lett.* **48** 926
Jain A, Lin C D and Fritsch W 1986 *Nucl. Instrum. Methods* B **24/25** 119
—— 1987a *Phys. Rev.* A **35** 3180
—— 1987b *Phys. Rev.* A **35** 2041
Kimura M and Lin C D 1985 *Phys. Rev.* A **32** 1357
Kimura M and Thorson W R 1981 *Phys. Rev.* A **24** 1780
Madison D H and Winters K M 1981 *Phys. Rev. Lett.* **47** 1885
Rapp D and Dinwiddie D 1972 *J. Chem. Phys.* **57** 4919
Schöller O, Briggs J S and Dreizler R M 1986 *J. Phys. B: At. Mol. Phys.* **19** 2505
van Wyngaarden W L and Walters H R J 1985 *J. Phys. B: At. Mol. Phys.* **18** L689
Walters H R J 1987 Private communication
Westerveld W B, Ashburn J R, Cline R A, Stone C D, Vanderburgt P J M and Risley J S 1987 *Nucl. Instrum. Methods* B **24/25** 224
Winter T G, Dutta C M and Lane N F 1985 *Phys. Rev.* A **31** 2702
Winter T G and Lin C D 1984 *Phys. Rev.* A **29** 567